Unnamed Systems, Vol. 5, No. 3 (2017) 141–157

DOI: 10.1142/S2301385017400039

Unmanned Systems
http://www.worldscientific.com/worldscinet/us

Observability Conditions for Switching Sensing Topology for Cooperative Localization

Anusna Chakraborty[*,‡], Sohum Misra[*,§], Rajnikant Sharma[*,¶], Clark. N. Taylor[†]

[*]*Aerospace Engineering and Engineering Mechanics, University of Cincinnati, Cincinnati, OH 45221, USA*

[†]*Sensors Directorate, AFRL, Wright Patterson Air Force Base, Dayton, OH 45433, USA*

In this paper, we solve a discrete-time bearing-only cooperative localization problem for a team of autonomous vehicles with a special focus on switching sensing topology. A centralized Extended Kalman Filter (EKF) is used for jointly estimating position and heading of all the vehicles using local motion and relative bearing measurements. We derive discrete-time conditions for switching relative sensing topology. Furthermore, we use cooperative synchronization for generating vehicle paths that satisfy the observability conditions. The conditions are verified through simulation and experimental results.

Keywords: Multi-agent systems; cooperative localization; extended kalman filter; time-varying topology; switching observability.

1. Introduction

With the advent of miniaturized sensors, single board computers, and batteries, it is possible to realize mobile sensor network of autonomous vehicles where geographically distributed sensors of limited capability work together to achieve a desired objective. One such important objective is vehicle localization. In a mobile sensor network, vehicles can share their local sensor information that consists of vehicle motion and relative position measurements (as shown in Fig. 1, to jointly estimate each vehicle's position and heading. Cooperative localization has received lots of attention [1–8] over the last decade because it offers several advantages over single vehicle localization such as increased localization accuracy, robustness, sensor coverage, flexibility, and more information. Cooperative localization has been used for navigation of unmanned aerial vehicles, [9–11] underwater vehicles [12], ground vehicles [13], and a combination of air and ground vehicles [14]. Furthermore, cooperative localization has been used for cooperatively tracking a target in GPS-denied environments [15] and co-operative-timing mission [16].

The cooperative localization problem can be solved using different estimation approaches such as Extended Kalman Filter (EKF) [17], Maximum Likelihood Estimator [18], Maximum *a Priori* (MAP) [19], and Factor Graphs [20]. For the cooperative localization estimates to be bounded, irrespective of the type of estimation technique, the system should be observable [21]. Observability is associated with the ability to distinguish different states given the sensor information. A nonlinear observability analysis for bearing-only cooperative localization for continuous-time case has been done in [22]. It has been shown for continuous-time case that the states of all the vehicles are observable if each vehicle node in the relative position measurement graph (RPMG) has path to two different known landmarks. Observability conditions, obtained in [22] are sufficient, requires constant connected RPMG topology that needs to be satisfied at all time instants. However, in real-time

Received 23 September 2016; Revised 31 May 2017; Accepted 1 June 2017; Published 1 August 2017. This paper was accepted for publication in the Special issue on Aerial Robotics: Success Stories of Today and Hopes of Tomorrow. Guest Editors: Farrokh Janabi Sharifi, Youmin Zhang, Hossein Bonyan Khamseh and Howard Li.
Email Addresses: [‡]*anusna90@gmail.com*, [§]*misra.sohum@gmail.com*, [¶]*rajnikant.sharma@uc.edu*

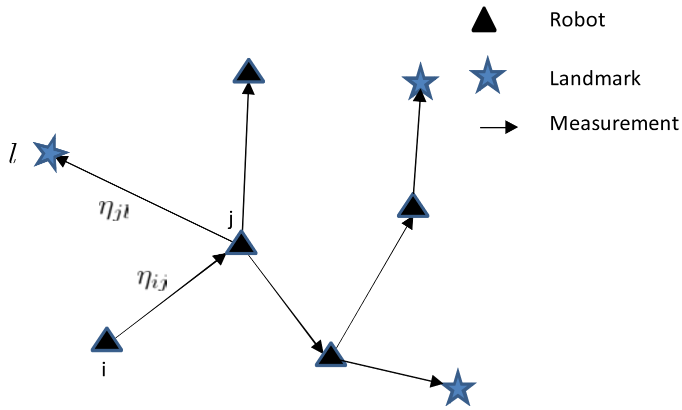

Fig. 1. Relative position measurement graph (RPMG) [17].

scenarios because of limited sensing range and field-of-view (FOV), the RPMG is not constant and have switching topology. Switching topology is best modeled as a discrete-time system and requires a nonlinear discrete-time observability analysis. So far, to the best of our knowledge, observability conditions for discrete-time cooperative localization problem for $n > 2$ are not derived in the existing literature.

Observability conditions are very critical for multi-agent systems' path planning. Vehicles should coordinate with each other while path planning to maintain the overall observability. A continuous-time cooperative path-planner to maintain observability has been demonstrated in [23]. In another work [24], a vehicle routing and landmark placement problem was solved such that the continuous-time observability conditions were satisfied. As mentioned earlier, the conditions derived in the continuous-time case are much harder to satisfy in real-time scenarios. However, it will be shown in this paper that discrete-time conditions are relaxed such that it can handle switching topology. For coordinated path planning to maintain discrete-time observability conditions, we use a cooperative synchronization algorithm as introduced in [25].

The main contributions of this paper are as follows:

- We derive observability conditions for discrete-time cooperative localization problem shown in Fig. 2 which are more relaxed than continuous-time case and are valid for switching relative-sensing topology.
- We use a cooperative synchronization algorithm to coordinate vehicle paths to periodically establish relative sensing topology required to keep the system observable.
- We validate the discrete-time observability conditions and the cooperative synchronization algorithm using both simulation and experimental results.

Rest of the paper is organized as follows. The discrete-time cooperative localization is formulated in Sec. 2 followed by discrete-time observability analysis in Sec. 3. Section 4 introduces the cooperative synchronization problem. Section 5 includes the simulation and hardware results followed by a discussion of the results. Finally, we present our conclusions and future work in Sec. 6.

2. Problem Formulation

Consider n vehicles moving in a horizontal plane with constant velocity in presence of l known landmarks as shown in Fig. 2. Equation of motion of the ith vehicle is given as

$$\begin{aligned} X_i(k+1) &= f_i(X_i(k), u_i(k)) \\ &= X_i(k) + T_s \begin{bmatrix} v_i(k)\cos\psi_i(k) \\ v_i(k)\sin\psi_i(k) \\ \omega_i(k) \end{bmatrix}, \end{aligned} \tag{1}$$

where $X_i(k) = [x_i(k)\ y_i(k)\ \psi_i(k)]^\top$ is state vector of ith vehicle with 2D position $[x_i(k),\ y_i(k)]$ and heading angle $\psi_i(k)$, T_s is sampling time, $u_i(k) = [v_i(k)\ \omega_i(k)]^\top$ is the input vector of the ith vehicle with velocity $v_i(k)$, and turn rate $\omega_i(k)$.

Each vehicle is equipped with a velocity and a turn rate sensor. Also, each vehicle has a sensor to measure bearing angle from the vehicles and landmarks that are in its sensing range. The bearing angle measured from the ith vehicle to the jth vehicle or landmark is given as

$$\begin{aligned} \eta_{ij}(k) &= h_{ij}(X_i(k), X_j(k)) \\ &= \tan^{-1}\frac{y_j(k) - y_i(k)}{x_j(k) - x_i(k)} - \psi_i(k) \\ i &= [1, \ldots, n], \quad j = [1, \ldots, n,\ n+1, \ldots, n+l], \end{aligned} \tag{2}$$

where n is the total number of vehicles and l is the total number of landmarks in the system.

The objective of cooperative localization problem is to jointly estimate the states of all the vehicles $X(k) = [X_1^\top(k), \ldots, X_n^\top(k)]^\top$ by using local vehicle motion and bearing angle information from all the vehicles. The cooperative localization problem can be represented by a Bayes Network as shown in Fig. 3 where the nodes are the current position of the vehicles at each time instant and the edges joining the nodes are the control inputs required to move the ith vehicle from position a to b. We use a Centralized EKF to estimate the required states because of its simplicity and the filtering process is sequential and online. The algorithm is detailed in Algorithm 1. In a centralized filter, all the vehicles send their local sensor information to a centralized node where an EKF is used to estimate all the vehicle states.

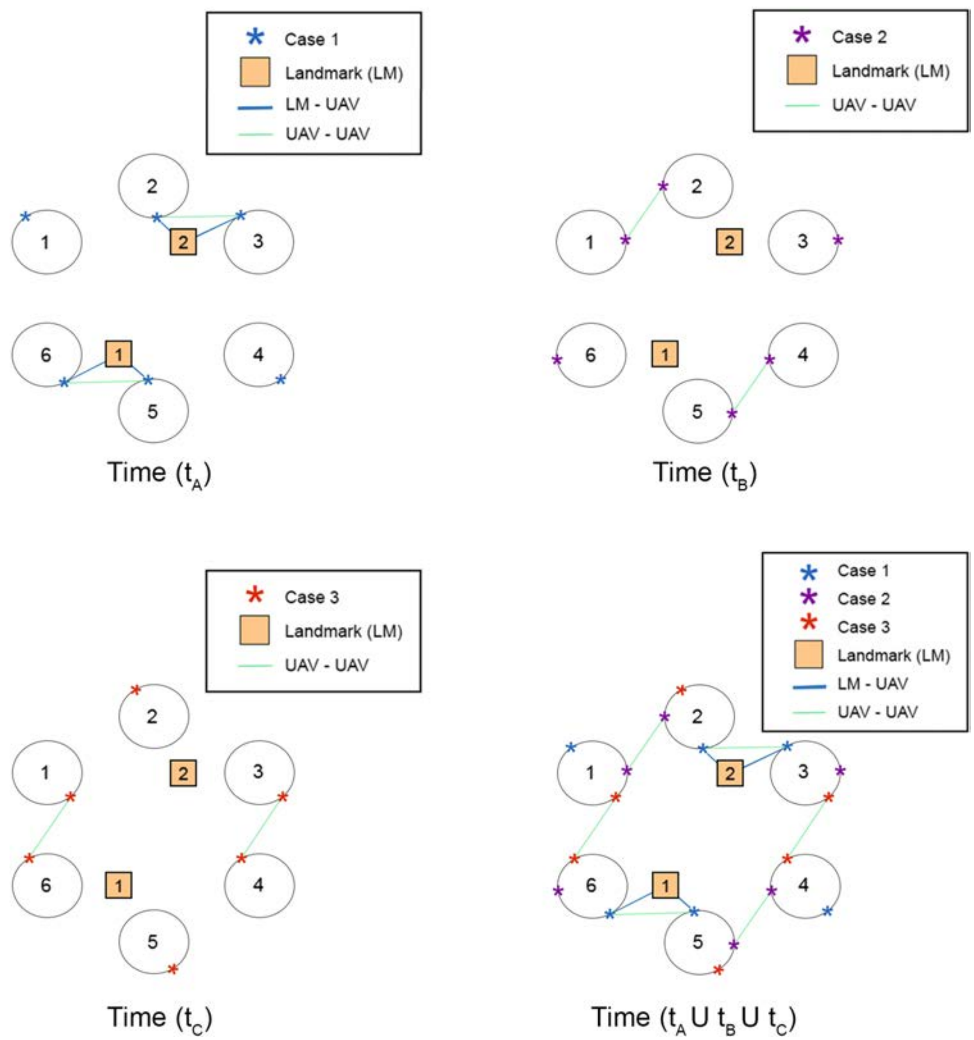

Fig. 2. A cooperative localization scenario.

In order to deploy a team of vehicles performing cooperative localization, it is very important that the system is observable to ensure bounded error in state estimates. If the system is observable, then the estimated and true states converge within a small bound and the states can be distinguished at different time intervals.

3. Nonlinear Discrete-Time Observability

In this section, we define the observability matrix for discrete-time system and then derive the sufficient conditions under which the discrete-time system is fully observable. The topology considered in this paper is switching and is not fixed. So the measurements are not continuous and hence we define discrete time observability.

For a discrete-time nonlinear system

$$X(k+1) = f(X(k), u(k)), \tag{3}$$

$$Z(k) = h(X(k)). \tag{4}$$

The observability matrix over a time period can be written as

$$O(k : k+\tau) = \begin{bmatrix} \frac{\partial h}{\partial X}(X(k)) \\ \frac{\partial h}{\partial X}(X(k+1))\Phi(k, k+1) \\ \vdots \\ \frac{\partial h}{\partial X}(X(k+\tau))\Phi(k, k+\tau) \end{bmatrix}, \tag{5}$$

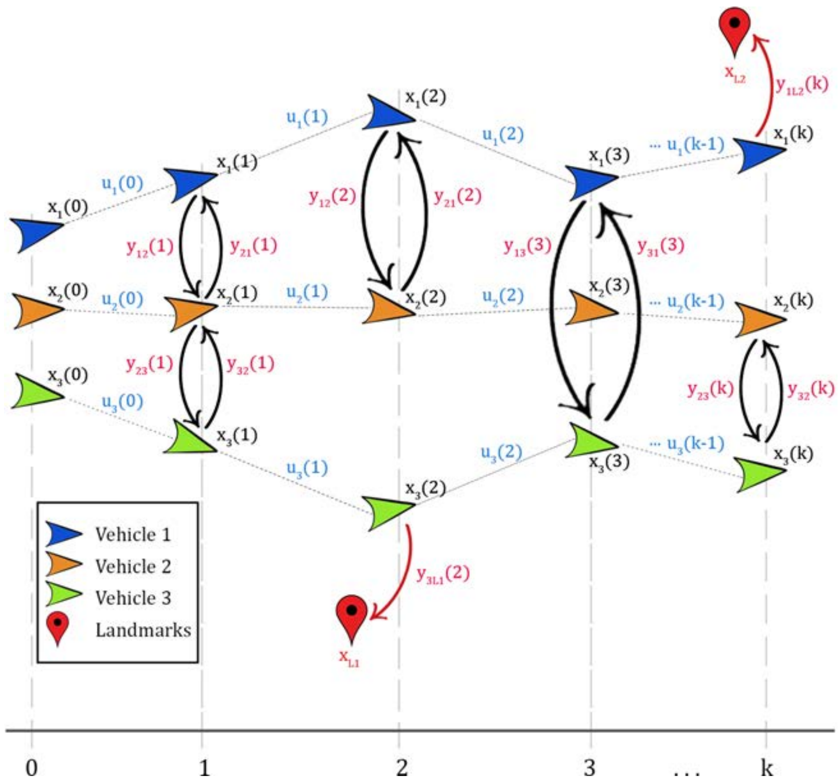

Fig. 3. Bayesian network representation of cooperative localization.

where

$$\Phi(k,k+1) = \frac{\partial f}{\partial X}(X(k),u(k)),$$
$$\Phi(k,k+\tau) = \Phi(k+\tau-1,k+\tau),\ldots,\Phi(k,k+1)$$

are transition matrices.

The observability matrix at different time steps are related as follows:

$$O(k,k+\tau) = \begin{bmatrix} O(k) \\ O(k+1)\Phi(k,k+1) \\ \vdots \\ O(k+\tau)\Phi(k,k+\tau) \end{bmatrix}, \qquad (6)$$

where $O(k) = \frac{\partial h}{\partial X}(X(k))$. The system is completely observable when $rank(O(k,k+\tau)) = n$.

From Eq. (2), we find

$$H_{ij}(k) = \frac{\partial h_{ij}(X_i(k),X_j(k))}{\partial X}$$
$$= [\mathbf{0_{3(i-1)}} \vdots\, H_{ij}^i(k) \vdots\, \mathbf{0_{3(j-1)-3i}} \vdots\, H_{ij}^j(k) \vdots\, \mathbf{0_{3(n-j)}}], \quad (7)$$

where

$$H_{ij}^i(k) = \left[\frac{-\Delta y_{ij}(k)}{R_{ij}^2} \;\; \frac{\Delta x_{ij}(k)}{R_{ij}^2} - 1\right],$$

and

$$H_{ij}^j(k) = \left[\frac{\Delta y_{ij}(k)}{R_{ij}^2} \;\; \frac{-\Delta x_{ij}(k)}{R_{ij}^2} \;\; 0\right] \; \forall j \in [1,n].$$

$H_{ij}^j(k)$ is not used $\forall j \in [n+1, n+l]$ due to the measurement being of a landmark of known location, so the landmark portion of the state does not depend on the state.

The system Jacobian for cooperative localization problem is given as

$$F(k) = \frac{\partial f}{\partial X}(X(k),u(k)) = \begin{bmatrix} F_1(k) & 0 & 0 \\ 0 & \ddots & 0 \\ 0 & 0 & F_n(k) \end{bmatrix},$$

$$F_i(k) = \frac{\partial f_i}{\partial X_i}(X_i(k),u_i(k)) = \begin{bmatrix} 1 & 0 & -a_i(k) \\ 0 & 1 & b_i(k) \\ 0 & 0 & 1 \end{bmatrix},$$

where

$$a_i(k) = T_s v_i(k) \sin\psi_i(k),$$
$$b_i(k) = T_s v_i(k) \cos\psi_i(k).$$

Algorithm 1. Centralized Cooperative Localization

Initialize $\hat{X} = X_0$
For each sample time T_s :
for $i = 1$ *to* N **do** Prediction Step
$\hat{X} = \hat{X} + (\frac{T_s}{N})\ f(\hat{X}, u)$
$A = \frac{\partial f}{\partial X}\ f(\hat{X}, u)$
$P = P + (\frac{T_s}{N})\ (AP + PA^T + Q)$
end for
If bearing measurement to landmark is received **then bearing update**
for $j = 1$ to l (number of landmarks) **do**
$H_{l_{ij}} = \frac{\partial h(\hat{X},u)}{\partial X}$
$L_{l_{ij}} = PH_{l_{ij}}^T\ (R + H_{l_{ij}} PH_{l_{ij}}^T)^{-1}$
$P = (I - L_{l_{ij}} H_{l_{ij}})P$
$\hat{X} = \hat{X} + L_{l_{ij}}(y_{l_{ij}} - Z(\hat{X}, u))$
end for
end if
If relative bearing measurement to neighboring vehicle received **then relative bearing update**
for $k = 1$ to n (number of vehicles) **do**
if $i \neq k$ **then do**
$H_{ik} = \frac{\partial h(\hat{X},u)}{\partial X}$
$L_{ik} = PH_{ik}^T\ (R + H_{ik} PH_{ik}^T)^{-1}$
$P = (I - L_{ik} H_{ik})P$
$\hat{X} = \hat{X} + L_{ik}(y_{ik} - Z(\hat{X}, u))$
end if
end for relative with vehicle if available
end if

The observability matrix for cooperative localization can be written as

$$O(k : k+\tau) = \begin{bmatrix} H_{ij}(k) \\ H_{ij}(k+1)F(k) \\ \vdots \\ H_{ij}(k+\tau)F(k+\tau-1)\cdots F(k) \end{bmatrix}. \quad (8)$$

The above matrix can be rearranged and written as

$$O(k : k+\tau) = [O_{ij}(k : k+\tau)],\ \forall i \in [1, n],\ j \in [1, n+l]. \quad (9)$$

From the above equation, we can say that the overall observability can be constructed by stacking observability matrix of all the edges η_{ij} over $k : k+\tau$ where each measurement is referred back to time k. Next, we find how many linearly independent rows an edge contributes to the overall observability matrix.

Lemma 3.1. *The maximum rank of the observability matrix $O_{ij}(k : k+\tau)$ between two vehicles is three if at least three bearing measurements are taken at three different time instants between $k, k+\tau$ and if*

(1) $v_i > 0$ *and* $v_j > 0$.
(2) *The vehicles do not move along the straight line joining them.*
(3) $\psi_i(k) - \psi_j(k) \neq 0$.

Proof. If the above conditions are satisfied then there exists an invertible matrix E_{ij} (details in Appendix) such that

$$E_{ij} O_{ij}(k, k+\tau) = [\mathbf{I_{3\times 3}}\ \ \bar{O_{ij}}], \quad (10)$$

where

$$\bar{O_{ij}} = \begin{bmatrix} -1 & 0 & \Delta y(k) \\ 0 & -1 & -\Delta x(k) \\ 0 & 0 & -1 \end{bmatrix}.$$

This implies that $rank(O_{ij}(k, k+\tau)) = 3$. □

Lemma 3.2. *The maximum rank of the observability matrix $O_{ij}(k : k+\tau)$ between a vehicle and a landmark is two if at least two bearing measurements are taken at two different time instants between $k, k+\tau$ and if*

(1) $v_i > 0$
(2) *The vehicle is not moving along the line joining the vehicle and the landmark.*

Proof. If the above conditions are satisfied, then there exists an invertible matrix E_{ij} (details in Appendix) such that

$$E_{ij} O_{ij}(k, k+\tau) = \begin{bmatrix} \bar{O_{ij}} \\ \mathbf{0(1\times 3)} \end{bmatrix},\ \forall i \in [1, n],\ j \in [n+1, n+l], \quad (11)$$

where

$$\bar{O_{iL}} = \begin{bmatrix} 1 & 0 & \Delta y(k) \\ 0 & 1 & -\Delta x(k) \end{bmatrix}.$$

This implies that $rank(O_{ij}(k, k+\tau)) = 2$. □

The above two lemmas show that the number of linearly independent rows in "(10)" and in "(11)" contributed by two types of edges are same as obtained in continuous-time case [22]. In fact, they span the same observable space with same basis. Using this, we can state the following theorem for the overall observability of discrete-time nonlinear cooperative localization problem. The proof of the following theorem can easily drawn from [22].

Theorem 3.3. *The overall system given by* "(1)" *is completely observable* (*i.e.* $rank(O(k, k+\tau)) = 3n$), *if the*

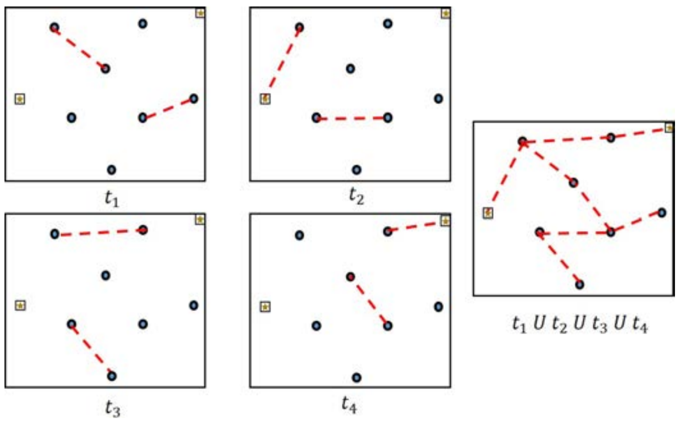

Fig. 4. Union of RPMG's to form a connected graph.

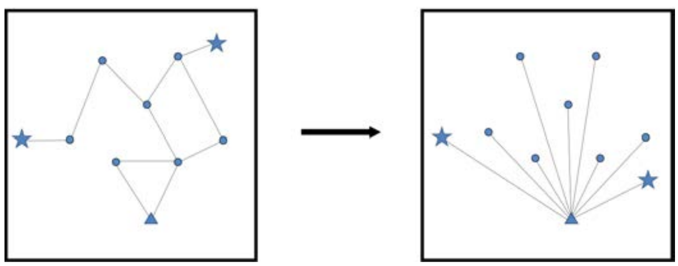

Fig. 5. Conversion of a RPMG to a two-level tree [22].

union of RPMGs at different time instants as shown in Figs. 2 *and* 4 *is connected and graph has at least two known landmarks and each edge between two vehicle satisfies conditions in Lemma* 3.1 *and edge between a vehicle and a landmark satisfies condition from Lemma* 3.2.

Proof. Let us consider a union of RPMGs with n vehicle nodes and m landmark nodes. In this graph, we only consider edges that satisfy Lemma 3.1 and Lemma 3.2. If this graph is connected, then similar to [22] it can be converted to a two-level tree as shown in Fig. 5. There are $n-1$ vehicle to vehicle edges contributing $3(n-1)$ linearly independent rows to the observability matrix. Also there are m vehicle to landmark edges which contributes additional three linearly independent rows for $m \geq 2$ resulting in $rank(O) = 3n$. □

4. Automated Synchronization with Cooperative Localization

In this section, an autonomous synchronization problem (Fig. 6) is formulated to maintain observability conditions as stated in Theorem 3.3. Consider n vehicles moving on circular path of same or different radii. The center of orbits are chosen such that the minimum distance between two vehicles is less than the sensing range. The problem is to cooperatively compute initial position and heading of vehicles such that RPMG connectivity is maintained periodically. The vehicles may move in either clockwise (CW) or anti-clockwise (ACW) direction, or the trajectories of the vehicles may be a combination of both with increased complexity of the system. However, the alternating combination of CW and ACW is more robust for our case as it allows more number of links between neighboring pairs to form simultaneously which reduces the time interval between communications. Conditions for maintaining periodic connectivity are adapted from [25] and are extended for nonbipartite connections. The two possible cases are discussed below.

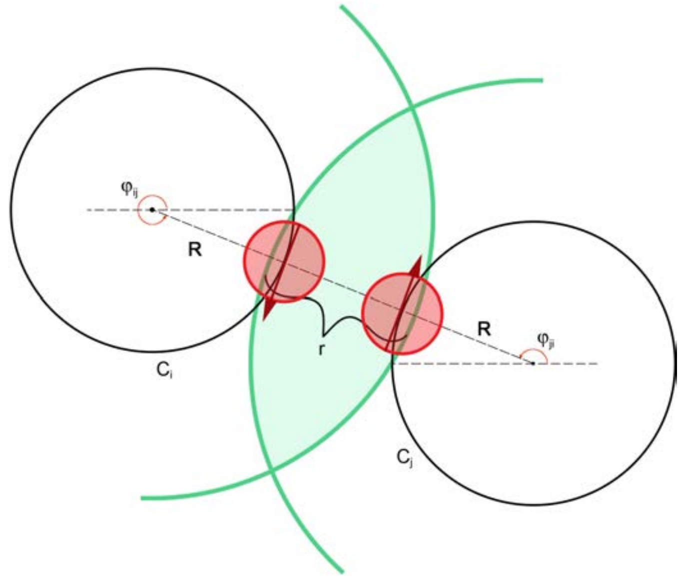

Fig. 6. Synchronization of two robots for maintenance of cyclic observability. [25]

4.1. *Same direction*

In this case, all vehicles move in the same direction, clockwise (CW) or anti-clockwise (ACW). In this paper, we consider that all the vehicles move in ACW direction without loss of generality. When the initial heading (with respect to the x-axis) of the first vehicle is known, the algorithm generates the initial heading of all other vehicles in a sequential manner.

The relationship between the initial heading of the ith and $(i+1)$th vehicle are computed in the following theorem.

Theorem 4.1. *Consider a RPMG $G(r) = (V, E(r))$ where the vehicles are traveling in the same direction in circular* *trajectories having the same angular velocity ω and communication distance r. Then the system is synchronized if and only if the graph is connected over a time period and the condition $\psi_j = \pi + \psi_i$ for every $(i, j) \in E(r)$ is satisfied.*

Proof. If an intermediate node cannot establish communication with its two adjacent neighbors, then there will be a situation where the nodes are clustered into several sub-graphs rather than one single connected graph. In such a scenario, the node n_i belonging to one sub-graph will fail to communicate (directly or indirectly) with node n_j belonging to another sub-graph and hence synchronization cannot be achieved.

If a graph $G(r)$ is connected end-to-end over a time period, then it can be divided into two categories or subsets. Each alternate node will fall in the same subset and a pair of such subsets (S1 and S2) are established. An arbitrary position ψ is assigned to all S1 vehicles. Any vehicle pair will be closest if the vehicles in S2 are assigned $\pi + \psi$ position. Let, V_i and V_j be a pair of neighboring nodes in the graph $G(r)$ connected by edge $E(r_{ij})$. Then, as per the above assumption, one belongs to S2 and the other belongs to S1 subset. Then, V_i and V_j are antipodal since angle of ψ_i (ϕ_{ij}) and angle of α_j (ϕ_{ji}) at any time instant are always separated by π. So, if same direction and angular velocity is maintained, the pair of neighboring nodes will always maintain antipodal positions and will repeatedly reach the sensing range after the same time interval provided there are no external disturbances. □

4.2. *Alternate direction*

For every $(i, j) \epsilon E(r)$ except for the nth and 1st vehicles, β_{ij} is the angle between the supporting line of the edge (i, j) in the connected graph G and the positive horizontal axis measured in counter-clockwise direction as shown in Fig. 7. In this case, the algorithm is modified to include information regarding the angle each subsequent neighboring trajectory is making with the previous one.

Theorem 4.2. *A RPMG be defined as $G(r) = (V, E(r))$ which consists of n vehicles. Every pair is scheduled to travel in alternate directions in circular trajectories of same or different radii with same angular velocity (ω) having communication distance r. Then the system is synchronized if and only if the graph is connected (any intermediate node has at least two connections with adjacent neighbors) and the condition $\psi_j = 2\beta_{ij} \pm \pi - \psi_i$ for every $(i, j) \in E(r)$ is satisfied.*

Proof. The necessary condition for Theorem 4.2 is the same as that of Theorem 4.1 as without inter-nodal connectivity, the trajectories of each vehicles will form

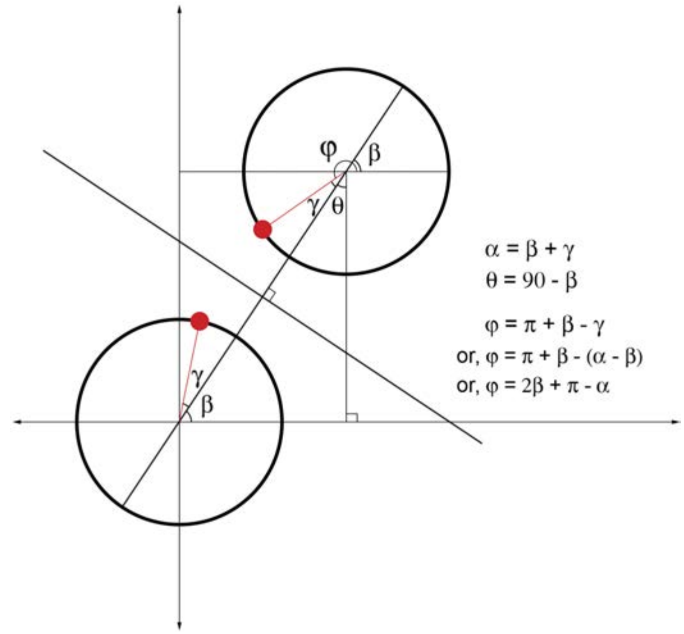

Fig. 7. Synchronization geometry for vehicles traveling in alternate direction.

disconnected sub-graphs. So, total synchronization will fail over the desired time period. The correct starting angle ensures that such scenario does not take place provided that there is no environmental or external noise.

If a graph $G(r)$ is connected end to end over a time period, then in this case, the starting position of the jth node will depend on the starting position of its previous node and the angle made by them with respect to the horizon. This is so because any two neighboring nodes should be at their closest position after 2π interval. As any given pair is traveling in alternate directions, node j should be the mirror image of node i (its previous node) with respect to the perpendicular bisector of the line joining the centers of their circular trajectories. If α_i is the angle of the previous node with respect to the horizon, β_{ij} is the angle made by the two nodes with respect to the horizon, then for the graph to establish end to end connectivity over a time period, the starting angle of the jth node $\psi_j = \beta_{ij} + \pi - (\psi_i - \beta_{ij})$ to establish and maintain periodic connectivity. □

The various synchronization cases may be summarized in Algorithm 2 where x_i, y_i are the center of the trajectories of the ith vehicle, R is the radius of the circle, ψ_i is the heading of the ith vehicle.

The main focus of the paper is application of the synchronization algorithm in cooperative localization which ensures that over a period of time, the RPMG is connected instead of a fully connected graph at each time instant. Figure 4 provides an example of cooperative localization with automated synchronization where each edge is established after a fixed time interval which is the total time period over which the RPMG shown in Fig. 1 is connected.

5. Results

5.1. *Simulation results*

The simulation results are based on the formation shown in Fig. 8 where the numbers inside the circle specify the sequence of the vehicles in the graph. Algorithm 2 is used to generate the initial heading for the vehicles in the group based on the heading of Vehicle 1. The sensor range, radius of the trajectory and vehicle velocity are user inputs and the angular velocity is calculated based on these inputs. The heading and trajectory information is fed to algorithm 1 to generate the estimated trajectories.

The simulation parameters used to test the validity of Theorem 3.3 are listed below:

- Initial pose uncertainty $= \{5\,\text{m}, 5\,\text{m}, 0.01\,\text{rad}\}$.
- Bearing measurement noise $= 0.001$ rad.
- Velocity $= 4$ m/s.
- Radius of trajectory $= 20$ m.
- Sensor range $= 50$ m
- Angular velocity $= 0.2$ rad/s.
- Graph connectivity time $= 0$ s.

Figure 9 proves the switching observability condition. No noise has been added to the position and velocity measurements, but a very small constant noise has been added to the bearing measurement. Initial uncertainty is associated with all the three states. Figure 9 shows the error and 3σ bounds of Vehicle 1. It is seen that the errors converge to zero, which proves Theorem 3.3 that the system may not remain observable at a time instant but over a time interval, if it satisfies the conditions, then the group will remain observable. Vehicle 1 did not have any direct path to either of the landmarks.

Algorithm 2. Automated synchronization for periodic information exchange

1: Initialize x_i, y_i sensor range and R.
2 : $Input\ \psi\ for\ the\ 1^{st} vehicle.$
3: **for** $i = 1toN$ **do** synchronous phase calculation
4 : **If** all agents revolve in the same direction **then assign phase**
5 : $\phi_{i+1} = \pi + \phi_i$
6: **end if**
7 : **If** all agents revolve in alternate direction **then assign phase**
8 : $\phi_{i+1} = 2\beta_i - \phi_i \mp \pi$
9: **end if**
10: Determine initial positions
11 : $X_i = Rcos(\psi_i) + x_i$.
12 : $Y_i = Rsin(\psi_i) + y_i$.

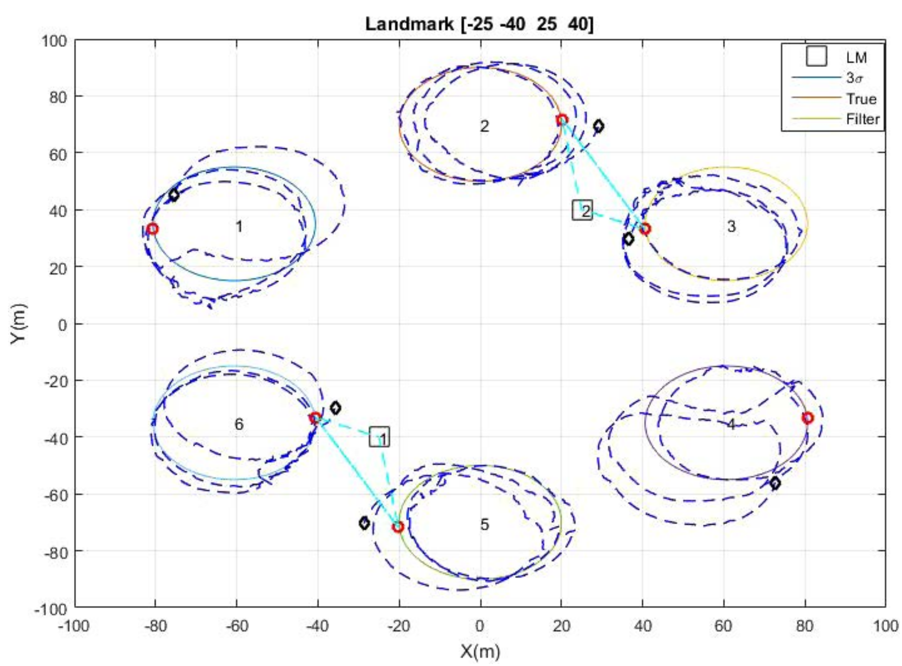

Fig. 8. Vehicle formation for cooperative localization with periodic synchronization.

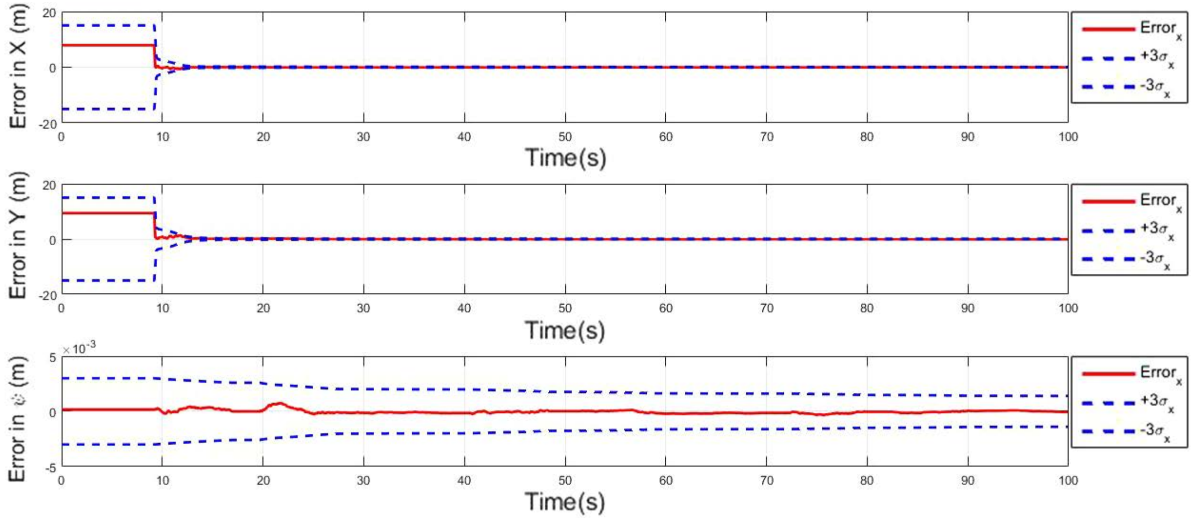

Fig. 9. Simulation-error plots for Vehicle 1 for ω = 0.2 without noise.

The parameters in the list below remains constant for all the following simulation cases:

- Initial pose uncertainty = $\{5\,\text{m}, 5\,\text{m}, 0.1\,\text{rad}\}$.
- Noise in velocity = 0.1 m/s
- Noise in gyro measurement = 0.01 rad/s.
- Bearing measurement noise = 0.1 rad.
- Radius of trajectory = 20 m.
- Sensor range = 50 m

5.1.1. *For $\omega = 0.2$ rad/s*

In this case, the velocity of the vehicles are 4 m/s. The connectivity period of the graph T_s is 31.4 s, which means that after every 31.4 s, the union of the RPMGs will yield a connected graph satisfying all conditions of Theorem 3.3. Figure 10 refers to the error and 3σ bound of Vehicle 1. Although the time period is large, the errors converge to zero over time.

5.1.2. *For $\omega = 1.0$ rad/s*

In this case, the velocity of the vehicles are 20 m/s. The connectivity period of the graph T_s is 6.28 s. Figure 11 refers to the error and 3σ bound of Vehicle 1. As seen from Table 1, this is the best case and it will be explained in detail further down this section.

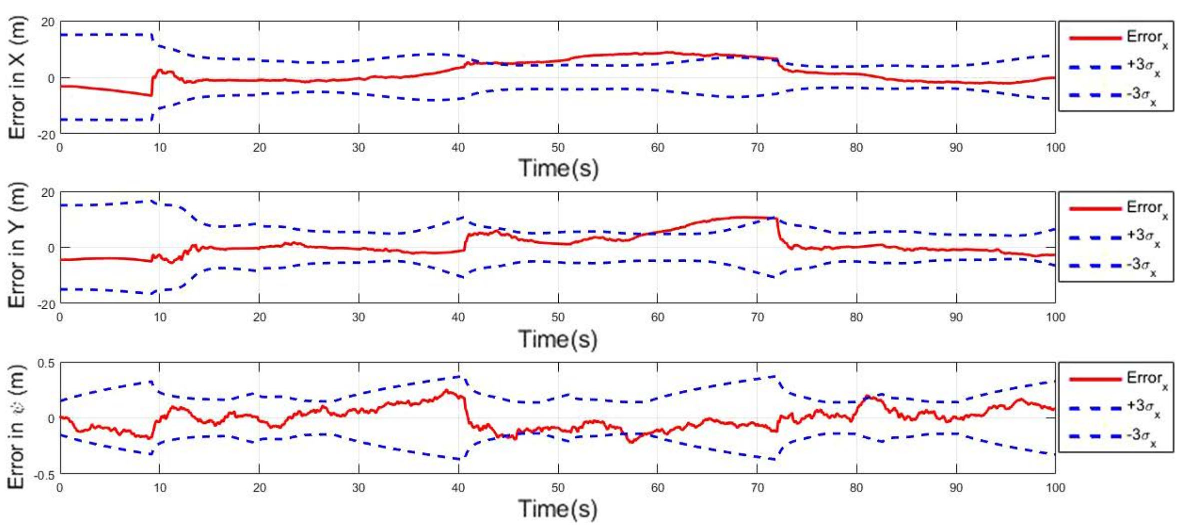

Fig. 10. Simulation-error plots for Vehicle 1 for ω = 0.2 with noise.

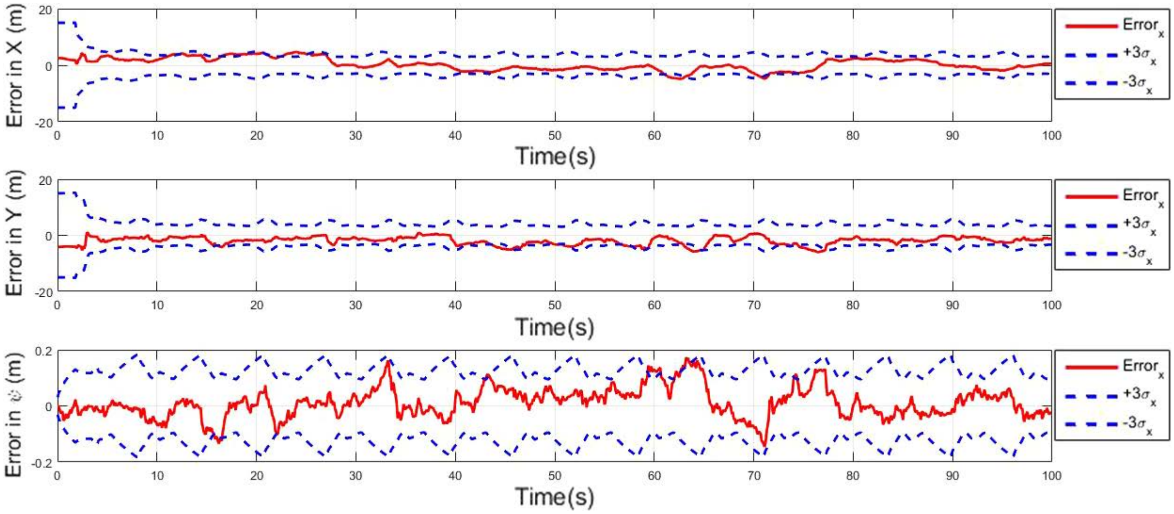

Fig. 11. Simulation-error plots for Vehicle 1 for ω = 1.0 with noise.

Table 1. Simulation Results — RMS position errors (in meters) for all vehicles with various ω values.

	Veh 1		Veh 2		Veh 3		Veh 4		Veh 5		Veh 6	
Values of ω	p_n	p_e	p_n	p_e	p_n	p_e	p_n	p_e	p_n	p_e	p_n	p_e
ω = 0.2	5.11	4.58	4.69	1.81	2.85	5.26	7.62	5.38	3.64	1.58	2.17	2.72
ω = 0.4	2.78	5.65	2.33	1.46	1.63	1.65	1.41	3.58	3.19	1.66	1.94	2.65
ω = 0.6	2.01	1.67	1.55	0.83	1.47	1.94	3.64	2.59	2.29	1.30	1.38	1.73
ω = 0.8	2.96	5.00	2.29	1.73	1.42	2.12	3.11	3.11	3.16	1.98	1.59	3.31
ω = 1.0	2.19	2.44	2.15	1.57	1.50	1.89	1.33	3.28	1.50	1.31	1.38	1.48
ω = 0.2 (**connected at each instant**)	0.49	1.36	0.95	0.53	0.69	0.67	1.20	0.70	2.39	1.59	1.37	1.27

5.2. *Hardware results*

The automated synchronization of the robots with switching observability has been implemented on Utah State University's Robust Intelligent Sensing Control Multi-Agent Analysis Platform (RISC MAAP). The hardware experiment comprises of four 3pi Polulu [26] ground robots (as seen in Fig. 13) following circular trajectories based on trajectory shaping algorithm. The indoor motion capture system (Cortex software by Motion Analysis — MoCap) comprises of 16 infrared cameras which are capable of detecting custom marker templates to triangulate the position and the heading of the robot with respect to the origin of the room and provides results in the accurate to 10 mm. The experiment is setup (see Fig. 12) based on the Robot Operating System (ROS) [27] which is an open source software that contains packages to map communication between the arduino on the robot and the ground computer via Xbee modules [28] in a master–slave mode to prevent overlap of

Table 2. Simulation Results — Average error for different values of ω.

Values of ω	p_n(m)	p_e(m)
$\omega = 0.2$	4.38	3.55
$\omega = 0.4$	2.21	2.78
$\omega = 0.6$	2.06	1.68
$\omega = 0.8$	2.12	2.87
$\omega = 1.0$	1.68	1.99

Table 3. Hardware Results — RMS errors for the 3pi robots $\omega = 0.8$ rad/s.

Vehicle no.	p_n(m)	p_e(m)
Vehicle 1	0.6216	0.6172
Vehicle 2	0.1896	0.2565
Vehicle 3	0.2336	0.1160
Vehicle 4	0.2046	0.1891

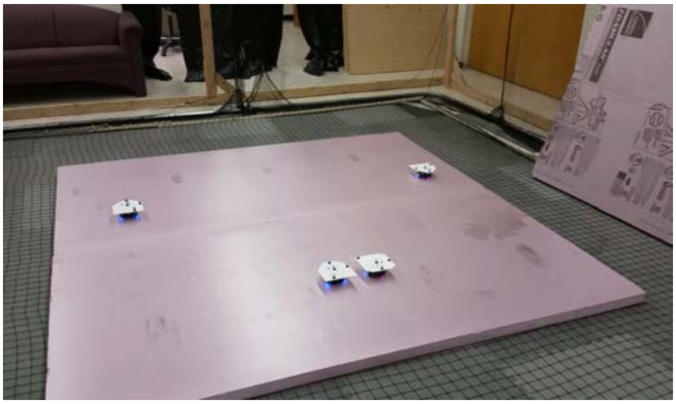

Fig. 12. The experimental setup in the RISC Lab with four 3pi robots-https://www.youtube.com/watch?v=Uf3_sCSkmfw.

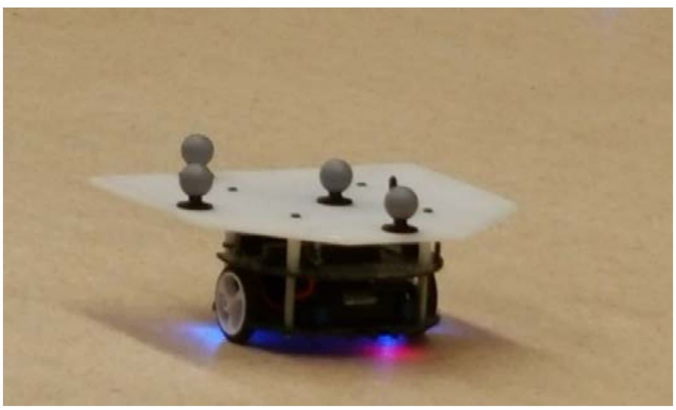

Fig. 13. A close up view of the 3pi robots.

commands sent. Based on the calibration of the cameras, the parameters setup for the hardware experiment is as follows:

- Initial pose uncertainty $= \{0.2\,\text{m}, 0.2\,\text{m}, 0.01\,\text{rad}\}$.
- Bearing measurement noise $= 0.05\,\text{rad}$.
- Velocity $= 0.4\,\text{m/s}$.
- Radius of trajectory $= 0.5\,\text{m}$.
- Sensor range $= 45\,\text{cm}$
- Angular velocity $= 0.8\,\text{rad/s}$.
- Graph connectivity time $= 7.85\,\text{s}$ (This is an approximate value and due to external noise in the hardware system this may vary between 7 to 9 s).

Remark 5.1. The relative measurements in this case has been obtained by adding noise to the data received from the MoCap system. The uncertainty in initial pose as well as the noise added to the bearing measurement and velocity is based on the tuning of the system.

Note: The last row in Table 1 gives the result for instantaneous observability when the connectivity time T_s goes to zero.

Table 1 reflects the variation of Root Mean Square (RMS) error in position with change in the angular velocity ω. For the case $\omega = 0.2$ rad/s, the table shows very high position errors but the errors are bounded by the 3σ limits as seen from Fig. 10. The connected graph is obtained after every 31.4 s which means that for some period of time in that cycle there is no connection between any vehicles. But as seen from Figs. 10 and 11, the errors converge to zero which means that the system is observable after every 31.4 s.

For increasing value of ω, the connectivity time decreases and hence the errors decrease. For $\omega = 1\,\text{rad/s}$, the

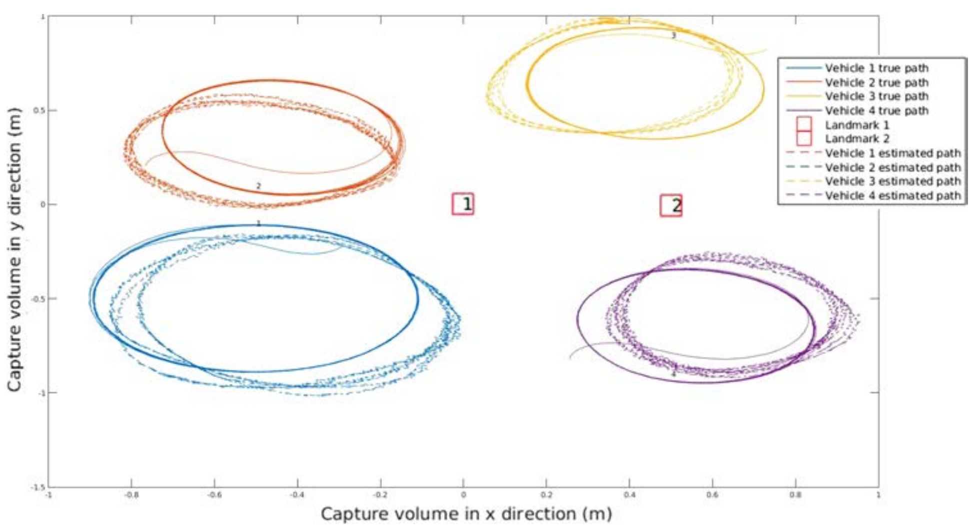

Fig. 14. Hardware — The true vs estimated trajectory for four robots.

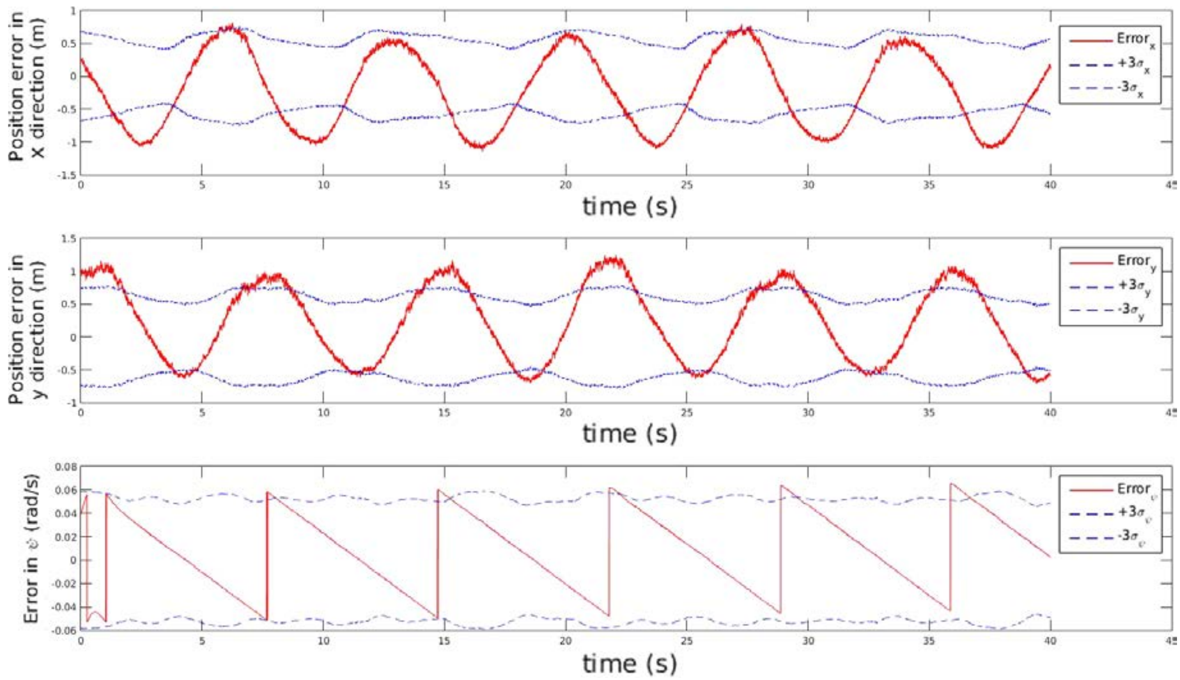

Fig. 15. Hardware — Position errors for Vehicle 1.

errors are lowest as the connectivity time is the lowest at 6.28 s. As the connected RPMG can be formed at a lesser time interval, the determinant of the observability matrix increases leading to low errors.

The last row in Table 1 shows the RMS errors in position if the graph was connected at all time instants. Even with $\omega = 0.2$ rad/s, the errors are very low. This is because the system is observable at all times, but in practical mission

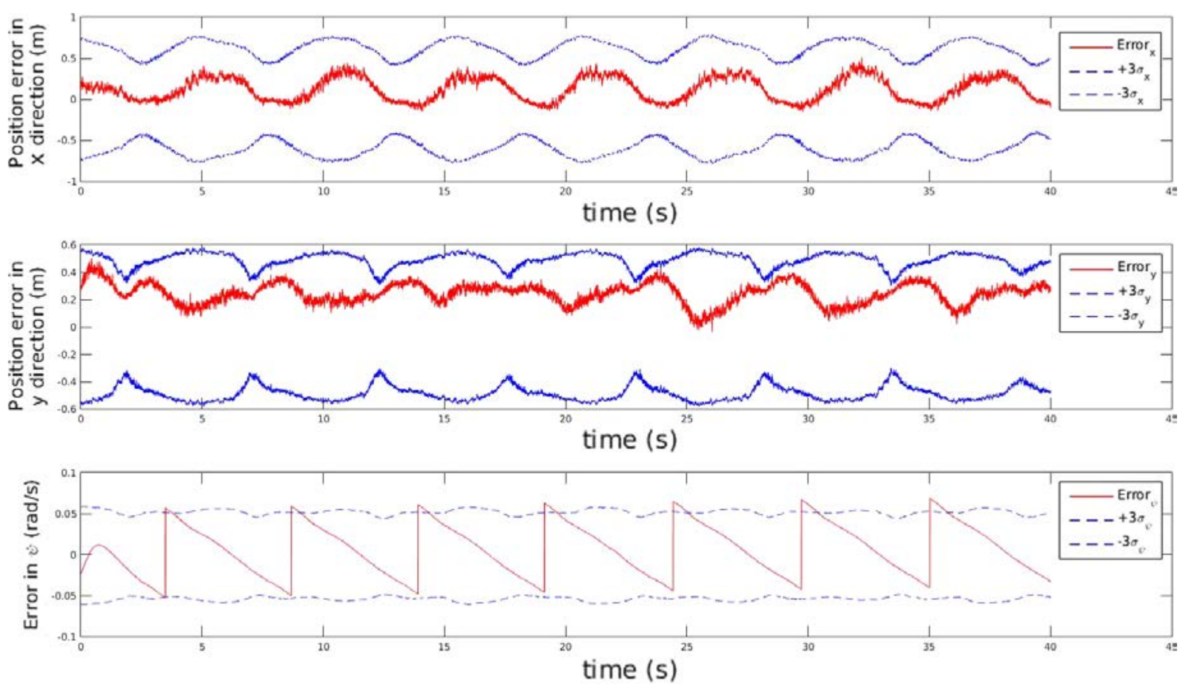

Fig. 16. Hardware — Position errors for Vehicle 2.

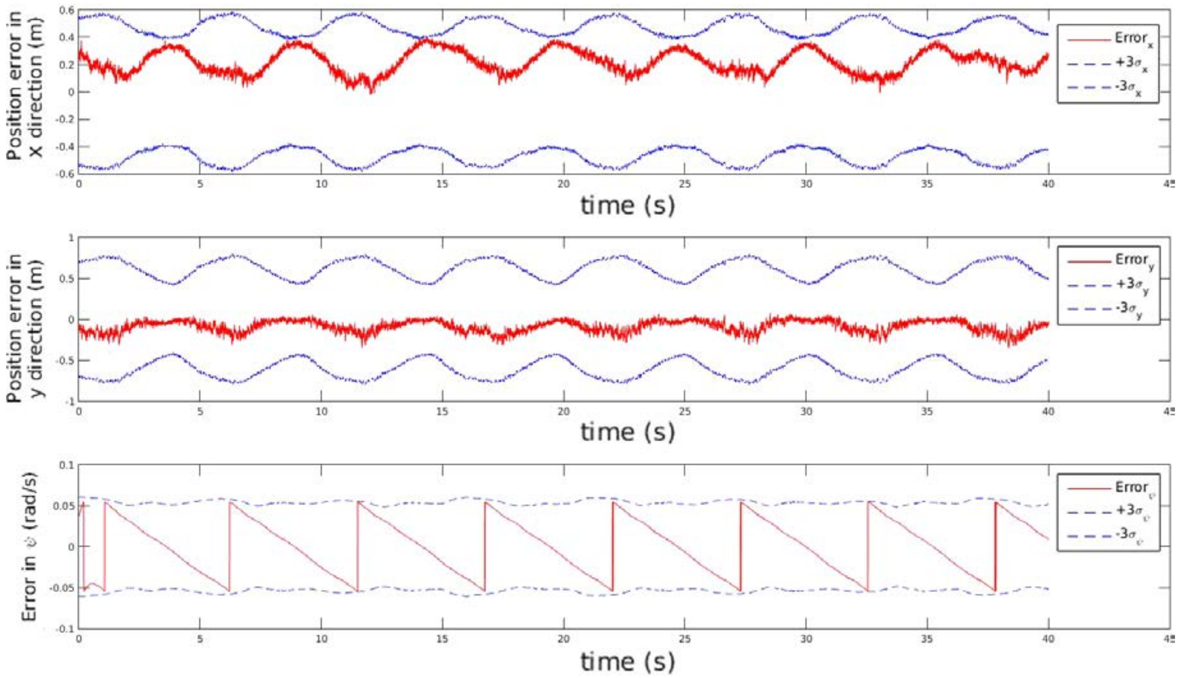

Fig. 17. Hardware — Position errors for Vehicle 3.

scenarios, this will be a very rigid condition to maintain. Hence, as long as the errors are within acceptable range, the system will remain observable over the time period.

The average error for the whole group is summarized in Table 2.

This table supports the findings from Table 1 and shows that with the increase in values of ω, the localization errors improve with the lowest error obtained at $\omega = 1$ rad/s.

The RMS errors for the results from hardware setup is given in Table 3.

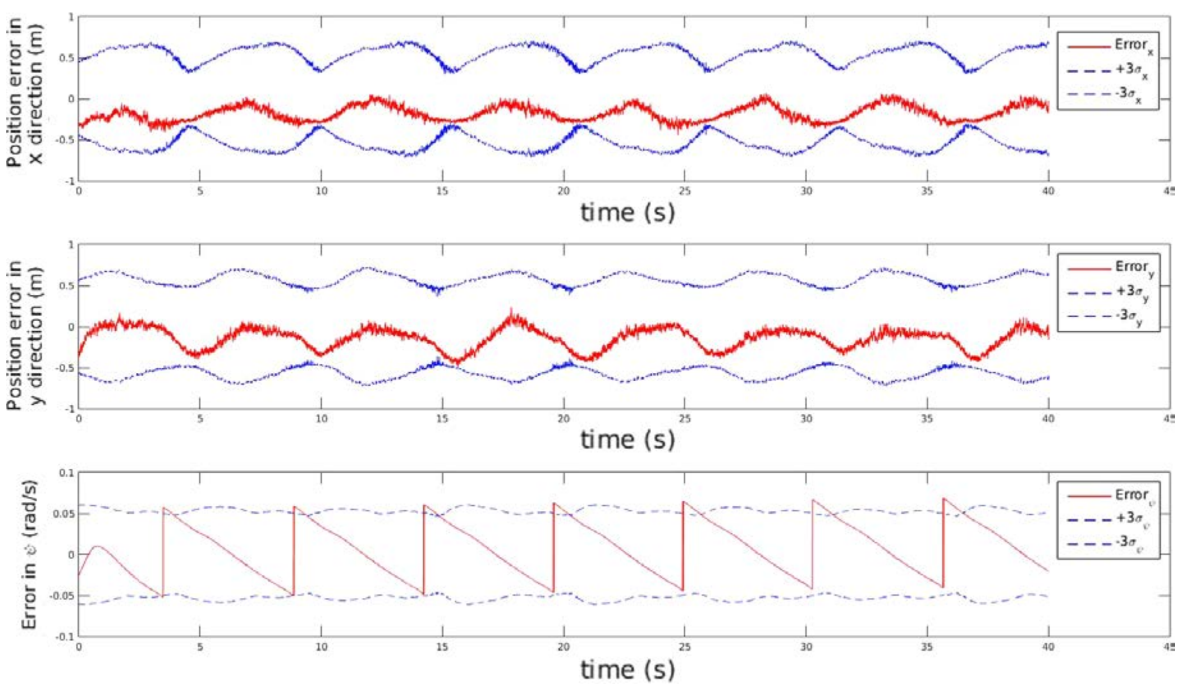

Fig. 18. Hardware — Position errors for Vehicle 4.

The graphs obtained from the hardware setup (Figs. 14–18) shows that the localization errors are bounded within the 3σ range. Uneven surface and occasional interference in the IR cameras contributes to some errors in the path of the vehicles. So, the outcome of the hardware experiment corroborates the simulation results.

6. Conclusions and Future Work

The results from the combination of cooperative localization with automated synchronization shows that for sufficiently long periods of time, if the union of RPMGs satisfies all the conditions in Theorem 3.3, then the system will remain observable even if the group does not maintain observability at every time instant. Synchronization amongst the vehicles ensures periodic communication which aids in creating a connected graph after a certain defined time interval. Landmark placement also plays an important factor in maintaining observability.

Algorithms 1 and 2 are applicable to any type of unmanned vehicle. The synchronization algorithm can be extended to account for different velocities or varying radii for circular trajectories. Additionally, the algorithm can be modified to be applicable for any nonuniform paths. A closed loop controller can be added to the synchronization algorithm to deal with external disturbances that might have been caused due to various factors such as wind gusts, sensor failure and vehicle failure.

Acknowledgments

This work is funded by NSF-IIS Robust Intelligence Award # 1526551. This paper cleared for public release, #88ABW-2016-5906.

Appendix A

The detailed proof for Lemmas 3.1 and 3.2 are given in this section.

A.1. *Proof of Lemma 3.1*

The general form of the observability matrix between two vehicles is given by Eq. (9). The expanded form of the observability matrix is given as

$$O_{ij}(k,k+\tau) = [O^1_{ij}(k,k+\tau) \vdots\, O^2_{ij}(k,k+\tau)], \tag{A.1}$$

where

$$O^1_{ij}(k,k+\tau) = \begin{bmatrix} \frac{-\Delta y(t_1)}{R(t_1)^2} & \frac{\Delta x(t_1)}{R(t_1)^2} & -1 \\ \frac{-\Delta y(t_2)}{R(t_2)^2} & \frac{\Delta x(t_2)}{R(t_2)^2} & \frac{a_i \Delta y(t_2)}{R(t_2)^2} + \frac{b_i \Delta x(t_2)}{R(t_2)^2} - 1 \\ \frac{-\Delta y(t_3)}{R(t_3)^2} & \frac{\Delta x(t_3)}{R(t_3)^2} & \frac{2a_i \Delta y(t_3)}{R(t_3)^2} + \frac{2b_i \Delta x(t_3)}{R(t_3)^2} - 1 \end{bmatrix},$$

and

$$O^2_{ij}(k,k+\tau) = \begin{bmatrix} \frac{-\Delta y(t_1)}{R(t_1)^2} & \frac{\Delta x(t_1)}{R(t_1)^2} & -1 \\ \frac{-\Delta y(t_2)}{R(t_2)^2} & \frac{\Delta x(t_2)}{R(t_2)^2} & \frac{a_j \Delta y(t_2)}{R(t_2)^2} + \frac{b_j \Delta x(t_2)}{R(t_2)^2} - 1 \\ \frac{-\Delta y(t_3)}{R(t_3)^2} & \frac{\Delta x(t_3)}{R(t_3)^2} & \frac{2a_j \Delta y(t_3)}{R(t_3)^2} + \frac{2b_j \Delta x(t_3)}{R(t_3)^2} - 1 \end{bmatrix}.$$

If $\psi_i(k+1) = \psi_i(k)$, then ψ_i is constant over t $\epsilon[k, k+\tau]$. The vehicles also have equal and constant velocity i.e. $v_i = v_j = V$.

The straight line joining the two robots can be written as $st_{ij}(k) = [\Delta x_{ij}(k), \Delta y_{ij}(k)]^T$. The heading vector for the ith vehicle is defined as $\psi^v_i = [\cos(\psi_i), \sin(\psi_i)]^T$. The vector perpendicular to the heading vector of the ith vehicle is given by $\psi^{v'}_i = [-\sin(\psi_i), \cos(\psi_i)]^T$. The vector along the line perpendicular to the straight line joining the two vehicles is given by $\psi^{v'}_i - \psi^{v'}_j$.

$$J^-_{ij} = st_{ij}(k)(\psi^{v'}_i - \psi^{v'}_j) = \Delta y_{ij}(k).\Delta^- C_\psi - \Delta x_{ij}(k).\Delta^- S_\psi, \tag{A.2}$$

$$D_\psi = \cos(\psi_i - \psi_j) - 1. \tag{A.3}$$

If the vehicles do not move along the straight line joining them, then $J^-_{ij} \neq 0$. Since the velocity of the vehicles are the same, so if $\psi_i \neq \psi_j$, then $D_\psi \neq 0$.

The elementary operation matrix E_{ij} which transforms the observability matrix O_{ij} can be written as

$$E_{ij} = \begin{bmatrix} E(1,1) & E(1,2) & E(1,3) \\ E(2,1) & E(2,2) & E(2,3) \\ E(3,1) & E(3,2) & E(3,3) \end{bmatrix}, \tag{A.4}$$

where

$$E_{ij}(1,1) = \frac{-R^2_k(\Delta X_{c\psi_j} - 3\Delta x(k) D_\psi - V^2) \times (C_{2\psi_j} - C_{2\psi_i})}{2V^2 J^-_{ij} D_\psi} - \frac{R^2_k(-T_{s\psi} + \Delta Y^-_c - 3V^2 \Delta^- C_\psi)}{2V^2 J^-_{ij} D_\psi},$$

$$E_{ij}(1,2) = \frac{-(2VD_\psi + R(k)^2 + 2(a_i\Delta x(k) + b_i\Delta y(k)))}{2V^2} \times \frac{(\Delta X_{c\psi_j} + \Delta^- Y_c + 2\Delta x(k)D_\psi - T_{s\psi})}{J_{ij}^- D_\psi},$$

$$E_{ij}(1,3) = \frac{(-8VD_\psi + R(k)^2 + 4VJ_{ij}^-)}{2V^2} \times \frac{(\Delta X_{c\psi_j} + \Delta^- Y_c + \Delta x(k)D_\psi + T_{s\psi})}{J_{ij}^+ D_\psi},$$

$$E_{ij}(2,1) = \frac{-R(k)^2(V^2(S_{2\psi_j} - S_{2\psi_i} - \Delta^- S_\psi))}{2V^2 J_{ij}^- D_\psi} - \frac{R(k)^2(-3V\Delta y(k) - T_{c\psi})}{2V^2 J_{ij}^- D_\psi},$$

$$E_{ij}(2,2) = \frac{-2V D_\psi + R(k)^2 + 2VJ_{ij}^+}{V^2 J_{ij}^- D_\psi},$$

$$E_{ij}(2,3) = \frac{-(-8V D_\psi + R(k)^2 + 4VJ_{ij}^+)}{2V^2} \times \frac{(\Delta Y_{s\psi_j} + \Delta^- X_c + \Delta y(k)D_\psi - T_{c\psi})}{J_{ij}^- D_\psi},$$

$$E_{ij}(3,1) = \frac{R(k)^2}{2V^2.D_\psi},$$

$$E_{ij}(3,2) = \frac{2VD_\psi - R(k)^2 - VJ_{ij}^+}{2V^2.D_\psi},$$

$$E_{ij}(3,3) = \frac{-8VD_\psi + R(k)^2 + 4VJ_{ij}^+}{2V^2.D_\psi},$$

where $T_{s\psi} = \Delta x(k)\Delta y(k)(\sin(\psi_i) - 2\sin(\psi_j))$, $T_{c\psi} = \Delta x(k)\Delta y(k)(\cos(\psi_i) - 2\cos(\psi_j))$, $J_{ij}^+ = (\Delta x(k)\Delta^- C_\psi + \Delta y(k)\Delta^- S_\psi)$, $\Delta^- C_\psi = \cos(\psi_i) - \cos(\psi_j)$, $\Delta^- S_\psi = \sin(\psi_i) - \sin(\psi_j)$, $\Delta^- Y_c = \Delta y(k)^2\Delta^- C_\psi$, $\Delta^- X_s = \Delta x(k)^2\Delta^- S_\psi$, $\Delta Y_{s\psi_j} = \Delta y(k)^2\sin(\psi_j)$ and $\Delta X_{c\psi_j} = \Delta x(k)^2\cos(\psi_j)$.

We already know that Eqs. (A.2) and (A.3) cannot be zero if the conditions stated in Lemma 3.1 is maintained. So, this shows that the matrix E is invertible.

The elementary transformation matrix that is obtained transforms the observability matrix $O_{ij}(k, k+\tau)$ as shown in Eq. (10) which verifies that the three rows of the matrix U are linearly independent and the maximum rank of the observability matrix is rank 3.

A.2. *Proof of Lemma 3.2*

The expanded observability matrix for an edge between a vehicle and landmark is given below

$$O_{ij}(k,k+\tau) = \begin{bmatrix} \frac{-\Delta y(t_1)}{R(t_1)^2} & \frac{\Delta x(t_1)}{R(t_1)^2} & -1 \\ \frac{-\Delta y(t_2)}{R(t_2)^2} & \frac{\Delta x(t_2)}{R(t_2)^2} & \frac{a_i\Delta y(t_2)}{R(t_2)^2} + \frac{b_i\Delta x(t_2)}{R(t_2)^2} - 1 \\ \frac{-\Delta y(t_3)}{R(t_3)^2} & \frac{\Delta x(t_3)}{R(t_3)^2} & \frac{2a_i\Delta y(t_3)}{R(t_3)^2} + \frac{2b_i\Delta x(t_3)}{R(t_3)^2} - 1 \end{bmatrix},$$

$\forall i \in [1,n],\ j \in [n+1, n+l]$

In the matrix above, the third row is already dependent on the second row and the next rows will all be dependent on the previous rows.

We assume $v(k+1) = v(k) = V$ and $\psi_i(k+1) = \psi_i(k) = \psi_i$ over t $\epsilon[k, k+\tau]$.

$$J_{iL}^- = st_{ij}(k)\psi_i^{v'} = \Delta y(k)cos(\psi_i) - \Delta x(k)sin(\psi_i), \quad \text{(A.5)}$$

where $st_{ij} = [\Delta x(k)\Delta y(k)]^T$ is the vector along the line joining the vehicle and landmark $\forall i \in [1,n],\ j \in [n+1, n+l]$. If the vehicle is not moving along the straight line joining itself to the landmark then $J_{iL}^- \neq 0$.

From the fact $E_{ij}O_{ij}(k, k+\tau) = U_{ij}$, we can find E_{ij} as given in Eq. (A.6).

$$E_{ij} = \begin{bmatrix} E(1,1) & E(1,2) & E(1,3) \\ E(2,1) & E(2,2) & E(2,3) \\ E(3,1) & E(3,2) & E(3,3) \end{bmatrix}, \quad \text{(A.6)}$$

where

$$E(1,1) = \frac{R(k)^2(\Delta x(k) + Vcos(\psi_i))}{VJ_{iL}^-},$$

$$E(1,2) = \frac{\Delta x(k)(V^2 + R(k)^2 + 2VJ_{iL}^+)}{VJ_{iL}^-},$$

$$E(1,3) = 0,$$

$$E(2,1) = \frac{R(k)^2(\Delta y(k) + V\,sin(\psi_i))}{VJ_{iL}^-},$$

$$E(2,2) = \frac{\Delta y(k)(V^2 + R(k)^2 + 2VJ_{iL}^-)}{VJ_{iL}^-},$$

$$E(2,3) = E(3,1) = E(3,2) = E(3,3) = 0.$$

If the conditions stated in Lemma 3.2 are satisfied, then E_{iL} is invertible. The transformation $E_{iL}O_{iL}(k, k+\tau)$ gives us U_{iL}.

$$U_{iL} = \begin{bmatrix} 1 & 0 & \Delta y_{iL} \\ 0 & 1 & -\Delta x_{iL} \\ 0 & 0 & 0 \end{bmatrix}.$$

So from Eq. (11) it can be verified that the maximum rank of the matrix is 2.

References

[1] R. Kurazume, S. Nagata and S. Hirose, Cooperative positioning with multiple robots, in *Proc. IEEE Int. Conf. Robotics and Automation*, 8–13 May 1994, pp. 1250–1257.

[2] R. Kurazume, S. Hirose, S. Nagata and N. Sashida, Study on cooperative positioning system (basic principle and measurement experiment), in *Proc. IEEE Int. Conf. Robotics and Automation*, Vol. 2, 22–28 April 1996, pp. 1421–1426.

[3] R. Kurazume and S. Hirose, Study on cooperative positioning system: Optimum moving strategies for CPS-III, in *Proc. IEEE Int. Conf. Robotics and Automation*, Vol. 4, 16–20 May 1998, pp. 2896–2903.

[4] A. Mourikis and S. Roumeliotis, Performance analysis of multirobot cooperative localization, *IEEE Trans. Robot. Auton. Syst.* **22**(4) (2006) 666–681.

[5] I. M. Rekleitis, G. Dudek and E. E. Milios, Multi-robot cooperative localization: A study of trade-offs between efficiency and accuracy, in *Proc. IEEE/RSJ Int. Conf. Intelligent Robots and System*, Vol. 3, 30 September–5 October 2002, pp. 2690–2695.

[6] S. I. Roumeliotis and G. A. Bekey, Distributed multirobot localization, *IEEE Trans. Robot. Autom.* **18**(5) (2002) 781–795. Available at http://ieeexplore.ieee.org/xpls/abs_all.jsp?arnumber=1067998.

[7] A. C. Sanderson, A distributed algorithm for cooperative navigation among multiple mobile robots, *Adv. Robot.* **12** (1998) 335–349.

[8] K. T. Song, C. Y. Tsai and C. H. C. Huang, Multi-robot cooperative sensing and localization, in *Proc. IEEE Int. Conf. Automation and Logistics (ICAL 2008)*, 1–3 September 2008, pp. 431–436.

[9] R. Sharma and C. N. Taylor, Cooperative navigation of MAVs in GPS denied areas, in *Proc. IEEE Int. Conf. Multisensor Fusion and Integration for Intell. Syst. (MFI 2008)*, 20–22 August 2008, pp. 481–486.

[10] R. Sharma and C. Taylor, Vision based distributed cooperative navigation for mavs in gps denied areas, in *Proc. AIAA Infotech @ Aerospace Conf.* (2009) Available at http://arc.aiaa.org/doi/pdf/10.2514/6.2009-1932.

[11] A. Chakraborty, C. N. Taylor, R. Sharma and K. M. Brink, Cooperative localization for fixed wing unmanned aerial vehicles, in *2016 IEEE/ION Position, Location and Navigation Symp. (PLANS)*. (IEEE, 2016), pp. 106–117.

[12] A. Bahr, J. J. Leonard and M. F. Fallon, Cooperative localization for autonomous underwater vehicles, *Int. J. Robot. Res.* **28**(6), (2009) 714–728. Available at http://ijr.sagepub.com/content/28/6/714.short.

[13] R. Sharma, S. Quebe, R. W. Beard, and C. N. Taylor, Bearing-only cooperative localization: Simulation and experimental results, *J. Intell. Robot. Syst.* **72**(3–4), 429, 2013.

[14] T. R. Wanasinghe, G. K. Mann and R. G. Gosine, Relative localization approach for combined aerial and ground robotic system, *J. Intell. Robot. Syst.* **77**(1) (2015) 113–133.

[15] R. Sharma, R. W. Beard, C. N. Taylor and D. Pack, Bearing-only cooperative geo-localization using unmanned aerial vehicles, in *American Control Conf. (ACC), 2012*. (*IEEE*, 2012), pp. 3883–3888. Available at http://ieeexplore.ieee.org/xpls/absl_all.jsp?arnumber=6315255.

[16] R. Sharma and S. Rathinam, Cooperative-timing attack with smart munitions using cooperative localization in contested environments: Formulation and centralized algorithm, *AIAA Infotech @ Aerospace, AIAA SciTech, At San Diego*, Volume: AIAA 2016-1712 January 2016. DOI: 10.2514/6.2016-1712. https://www.researchgate.net/publication/290779257_Cooperative-timing_Attack_with_Smart_Munitions_using_Cooperative_Localization_in_Contested_Environments_Formulation_and_Centralized_Algorithm

[17] R. Sharma, S. Quebe, R. W. Beard and C. N. Taylor, Bearing-only cooperative localization, *J. Intell. Robot. Syst.* **72**(3–4) (2013) 429–440.

[18] A. Howard, M. J. Matark and G. S. Sukhatme, Localization for mobile robot teams using maximum likelihood estimation, in *IEEE/RSJ Int. Conf. Intelligent Robots and Systems, 2002* Vol. 1. (IEEE, 2002), pp. 434–439.

[19] E. D. Nerurkar, S. I. Roumeliotis and A. Martinelli, "Distributed maximum a posteriori estimation for multi-robot cooperative localization," in *IEEE Int. Conf. Robotics and Automation, 2009 (ICRA'09)* (*IEEE*, 2009), pp. 1402–1409.

[20] E. D. Nerurkar and S. I. Roumeliotis, "Distributed map estimation algorithm for cooperative localization," Dept. of Comp. Sci. & Eng., University of Minnesota, Tech. Rep, (2008).

[21] G. Huang, N. Trawny, A. I. Mourikis and S. I. Roumeliotis, On the consistency of multi-robot cooperative localization, in *Robotics: Science and Systems* (2009), pp. 65–72.

[22] R. Sharma, R. W. Beard, C. N. Taylor and S. Quebe, Graph-based observability analysis of bearing-only cooperative localization, *IEEE Trans. Robot.* **28**(2) (2012) 522–529.

[23] R. Sharma, Observability based control for cooperative localization, in *IEEE, 2014 Int. Conf. Unmanned Aircraft Systems* (ICUAS, 2014) pp. 134–139.

[24] S. Rathinam and R. Sharma, A multiple vehicle path covering problem with localization constraints: Formulation and algorithms, in *2015 American Control Conference (ACC)* (*IEEE*, 2015), pp. 3746–3751.

[25] J. Diaz-Banez, E. Caraballo, M. Lopez, S. Bereg, I. Maza, and A. Ollero, "The synchronization problem for information exchange between aerial robots under communication constraints," in *Robotics and Automation (ICRA), 2015 IEEE International Conference on*. (*IEEE*, 2015), pp. 4650–4655.

[26] P. Robotics and Electronics, Pololu m3pi Robot with mbed Socket, available at https://www.pololu.com/product/2151, 2013, [Online; accessed on 26 April 2017].

[27] Robotics community, Robot Operating System, available at http://www.ros.org, 2000, [Online; accessed on 26 April 2017].

[28] Open Source Robotics Foundation, An Example rosserial xbee Network, available at http://wiki.ros.org/rosserial_xbee/Tutorials, 2012, [Online; accessed on 26 April 2017].

Anusna Chakraborty completed her Bacherlor's degree from St. Thomas' College of Engineering and Technology, Kolkata in 2012 and is currently pursuing her Ph.D. from University of Cincinnati from 2017. She is a Research Assistant in the Robust Intelligent Sensing and Control Lab (R.I.S.C Lab) at the university. Anusna is the author of three technical publications. Her research interests are Robotics, unmanned platforms, cooperative localization and applications of unmanned systems in various missions.

Sohum Misra completed his Bachelor's degree from Heritage Institute of Technology in 2015 and is pursuing Ph.D. from University of Cincinnati from 2017 where he is a Research Assistant in the R.I.S.C Lab. Sohum has three technical publications. His research interests are Sensor Integration, Robotics, Automation and Controls, Internet of Things. He is an IEEE student member.

Rajnikant Sharma received the B.E. degree in Electrical Engineering from the University of Rajasthan, Jaipur, India, in 2003, the M.E. degree in Aerospace Engineering from the Indian Institute of Science, Bangalore, India, in 2005, and the Ph. D. degree in Electrical Engineering in 2011 from the Brigham Young University, Provo, UT. From August 2013, he was with the Electrical and Computer Engineering Department at Utah State University, Logan, UT, as an Assistant Professor. Currently, he is an Assistant Professor in the Aerospace and Engineering Mechanics Department at the University of Cincinnati. In 2011–2013, he was a Postdoctoral fellow at Academy Center for UAS Research, US Air Force Academy, Colorado. From 2005–2007, he was a Scientist B at the Center for Airborne Systems, Defense Research and Development Organization, Ministry of Defense, Bangalore, India. His primary research interest are guidance, navigation, and control of unmanned aerial vehicles and multiple vehicle coordination, control, and localization. He is a member of the IEEE and AIAA.

Clark. N. Taylor received his Ph.D. degree from the University of California, San Diego in 2004. From 2004 to 2010, he worked as an Assistant Professor in Department of Electrical and Computer Engineering at Brigham Young University. He is a Senior Electronics Engineer at Sensors Directorate, United States Air Force Research Laboratory (AFRL). He has over 60 technical publications and his research emphasis is on exploitation for aerial imagery and the use of vision for navigation of autonomous vehicles.